# DETERMINING THE REFRACTIVE INDEX OF SCANDIUM OXIDE IN THE EUV USING KRAMERS-KRONIG ON THIN-FILM TRANSMISSION DATA

by

Jacqualine Dee Jackson

Submitted to Brigham Young University in partial fulfillment

of graduation requirements for University Honors

Department of Physics and Astronomy

April 2007

| | |
|---|---|
| Advisor: | Honors Representative: |
| David D. Allred | R. Steven Turley |
| Signature: _____ | Signature: _____ |

BRIGHAM YOUNG UNIVERSITY

DEPARTMENT APPROVAL

of a senior thesis submitted by

Jacqualine Dee Jackson

This thesis has been reviewed by the research advisor, research coordinator, and department chair and has been found to be satisfactory.

| | |
|---|---|
| Date | David D. Allred, Advisor |
| Date | Eric Hintz, Research Coordinator |
| Date | Scott Sommerfeldt, Chair |

# ABSTRACT

## DETERMINING THE REFRACTIVE INDEX OF SCANDIUM OXIDE IN THE EUV USING KRAMERS-KRONIG ON THIN-FILM TRANSMISSION DATA

Jacqualine Dee Jackson

Department of Physics and Astronomy

Bachelor of Science

It is difficult to measure the reflectance of thin films accurately in the extreme ultraviolet due to lack of precision instrumentation in this range and the effects of surface roughness. However, this has little effect on transmittance measurements. Whereas the real part of the refractive index is dependant on both transmittance and reflectance, the imaginary part can be determined from transmittance data alone. It is possible to use Kramers-Kronig analysis to calculate the real part if the imaginary part is known over a sufficiently broad range. We show that the delta calculated from reflection and transmission data without taking into account roughness may underestimate the real part of the refractive index of the scandium oxide samples we are studying by up to 40% near 270 eV.

# ACKNOWLEDGMENTS

I would like to thank my advisor, Dr. Allred, for guiding me in this project and for all the time he spent reading and editing my thesis. I would also like to thank Dr. Peatross and Dr. Rees for their input in the editing process and Dr. Turley for his input in the computational process. I also owe much thanks to Guillermo Acosta for providing me with the normalized data that I needed to complete my project. Additionally, I would like to thank my family for their love and support as I finish up my undergraduate career.

# Contents

# List of Figures

# Chapter 1

# Introduction

## 1.1 Applications of EUV optics

Extreme Ultraviolet (EUV) light is the portion of the electromagnetic spectrum ranging in photon energy from about 12 to 120 eV (which corresponds to wavelengths of $10-100$ nm and frequencies of $3000-30000$ THz). Whereas the reflective properties of materials in the visible portion of the spectrum have already been well-characterized, the optical properties of materials in the EUV range have not been as thoroughly researched. However, new applications for EUV light have caused greater motivation to study materials in this spectral range.

One such application is imaging of EUV emissions from singly ionized helium (about 30.4 nm) in the Earth's plasmasphere [1]. Such imaging is difficult because mirror technology in the EUV range is still in its early stages. Another application of EUV mirrors is in soft x ray/EUV laser systems that require multiple passes or redirection of the laser. These particular applications have motivated the BYU Thin Films Group to study the optical properties of several materials in the EUV range.

Just as there are dielectric mirrors (stacks of high and low index layers) in the

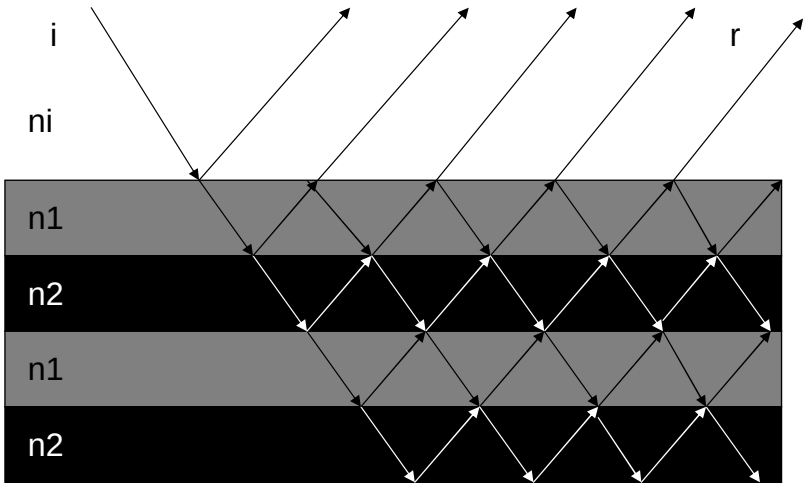


**Figure 1.1** Multilayer mirror stack – A multilayer stack is composed of alternating high and low index materials. This increases total reflection by coherently combining the reflection from each layer.

visible range of light, dielectric mirrors are also possible in the EUV range. These multilayer stacks increase reflectance in the EUV range when a bilayer composed mostly of a transparent material and a material with a high $\delta$ is repeated. ($\delta$ is related to the real part of the complex index of refraction, and $\beta$ is the imaginary part.) Uspenskii and coworkers suggested that scandium would be an exceptionally transparent layer in multilayer stacks around $35-50$ nm, reaching reflectances on the order of $67-72\%$ [2]. However, reflectances were only seen to be about half as high as expected. This disagreement between theory and experiment introduced a need to study more thoroughly the optical constants of scandium. Studies of these constants have been completed in the last two years, showing that scandium is more absorbing between $20-35$ eV than was previously believed [3].

Although various methods for obtaining optical constants exist, accurate determination of these constants in the EUV range is difficult. These difficulties arise from the strong EUV absorption of carbon, nitrogen, and oxygen, which are common sample surface and bulk contaminants. Changes in the $\delta$ and $\beta$ of a sample of an active

metal due to its reaction with atmospheric gases creates difficulties, but this can be lessened by using thoroughly oxidized samples, such as scandium oxide, instead of pure scandium [3].

The advantage of using scandium oxide instead of scandium is that it has already been oxidized and is, thus, less affected by the presence of oxygen, making measurements less sensitive and thus, more stable. However, scandium and scandium oxide should have different optical properties, due to the addition of oxygen features to the spectrum. Studying the optical constants of scandium oxide also provides useful information about the differences between pure metals and oxidized metals.

## 1.2 Optical Dispersion – Kramers-Kronig

Scientists have known about the dispersive properties of light for centuries. The most notable example of this phenomenon is the separation of white light into colors upon passing through a prism. Modern scientists know that this phenomenon is due to what is called the dispersion of the refractive index. This index is a ratio of the velocity of light in vacuum to its velocity in a given medium ($c/v$) and is a function of photon energy.

In the early 1800s, Cauchy deduced an equation relating the refractive index with wavelength. This equation gave accurate values in the case of normal dispersion, dispersion in spectral ranges far from any absorption lines, but it failed in regions of anomalous dispersion [4]. These sudden changes in the trend of the refractive index are due to a resonance in the medium. If the incident light wave has a frequency near that of the resonant frequency of the molecules in the medium, the light will excite the natural vibrations in these molecules. This causes an increase in absorption, due to the energy used to excite vibrations in the medium [4].

The theory of optical dispersion deals with the dependence of the complex index of refraction on wavelength. The index of refraction is normally defined as $n+i\kappa$. For our purposes, we define the index of refraction to be $\delta+i\beta$, where $\delta = 1-n$. The real part $\delta$ is determined by the phase velocity and the imaginary part $\beta$ is determined by the absorption. In 1926-1927 Kronig and Kramers showed that the real part can be expressed as an integral of the imaginary part and vice-versa [5]. This optical dispersion relation, which exists in several forms, is the basis of an analytic method known as Kramers–Kronig (KK) analysis.

Although $\delta$ and $\beta$ can both be calculated through measurements of absorption and phase shift, it is often difficult to accurately determine $\delta$ through such methods in the EUV and soft x ray ranges because surfaces are not ideal and instrumentation is not sufficiently advanced in this range [6]. However, it is usually possible to determine $\beta$ through such methods, as it can be calculated from transmission data alone, which varies less with angle. The KK relations can be written in a form that involves the atomic scattering factors $f_1$ and $f_2$. To use this form, it is necessary to note that $\delta$ and $\beta$ relate to $f_1$ and $f_2$ as follows:

$$\delta = \frac{n_a r_e \lambda^2}{2\pi} f_1^0(\omega) \tag{1.1}$$

$$\beta = \frac{n_a r_e \lambda^2}{2\pi} f_2^0(\omega) \tag{1.2}$$

where $n_a$ is the number of atoms per unit volume in the optical medium and $r_e$ is the classical electron radius [6].

The power of KK analysis, is that it is only necessary to determine experimentally the imaginary part of the atomic scattering factor, $f_2^0(\omega)$, to determine mathematically the real part, $f_1^0(\omega)$. The relationship between $f_2^0(\omega)$ and $f_1^0(\omega)$ is

$$f_1^0(\omega) = Z - \frac{2}{\pi} P_C \int_0^\infty \frac{u f_2^0(u)}{u^2 - \omega^2} du \tag{1.3}$$

$$f_2^0(\omega) = \frac{2\omega}{\pi} P_C \int_0^\infty \frac{f_1^0(u) - Z}{u^2 - \omega^2} du \tag{1.4}$$

where the first-order term $Z$ is the number of electrons per atom, $u$ is energy, and the $P_C$ indicates that only the non-divergent Cauchy principal part of the integral is to be considered [6]. It is important to note that these equations require integration across the full spectrum of frequencies.

It is possible to use the equation for $f_1^0(\omega)$ when $f_2^0(\omega)$ is only known across a portion of the spectrum if the range is sufficiently broad such that the integral converges [6]. However, it can often be difficult to obtain experimental data across a broad-enough range to meet this requirement, especially in areas surrounding absorption features. It would, therefore, be useful to understand the error introduced when one possesses only experimental data for a limited range of frequencies, for which the KK integral will not have converged to its infinite sum asymptote. This understanding might be achieved by applying KK analysis to this limited range of experimental data and comparing the KK $\delta$ calculations to our reflection and transmission (RT) $\delta$ calculations. The problem of a limited sum might be remedied by combining experimental data with the appropriate theoretical data above and below the experimental data. This calculation based on a combination of experimental and theoretical data can also be compared to the RT calculations. Such a study would allow researchers to apply KK analysis to smaller ranges of data by knowing what corrections to apply to their calculations.

## 1.3 Research Goals

This thesis describes the process of preparing scandium oxide thin films and taking optical measurements on these films. It also describes the application of KK analysis to experimental scandium oxide $\beta$ data over a given range to produce the real part

$\delta(\omega)$. This method gives us a way to evaluate data from an alternate method of calculating $\delta(\omega)$ via reflectance and transmittance data (RT $\delta$) [7]. We show that the KK method is unacceptable when we apply KK to experimental data over a finite range, but is reasonable when augmented with data provided by the Center for X-Ray Optics (CXRO) for the range above and below our experimental data. We are able to calculate $\delta(\omega)$ to within 40% relative to our previous method of calculating $\delta(\omega)$ by combining experimental and CXRO data. We believe this shows that our previous method underestimates the real $\delta$ by up to 40% at short wavelengths. Expanding the range for which theoretical and experimental data are known would decrease this percentage of error.

# Chapter 2

# Experimental procedure

## 2.1 Film preparation and characterization

The use of Kramers-Kronig analysis to obtain the real part $\delta$ of the index of refraction from the imaginary part $\beta$ is most useful when applied to experimental data, often collected from thin films. Knowing the dependability of such an analysis would allow researchers here at BYU to determine $\delta$ with more certainty than previously.

The thin films used for data collection in this project were produced by the BYU Thin Films Group through dc magnetron sputtering using a 99.9% pure scandium target manufactured by First Reaction. Results of chemical analysis performed by the manufacturer can be found in Table 2.1 [8]. The values listed are the results of dc arc optical emission spectroscopy, performed on the raw material used to make the target.

Thin film deposition is done in a vacuum chamber, which is pumped to high vacuum by use of a cryopump. The chamber generally reaches a base pressure of around 6 $\mu$Torr after approximately six hours of pumping. When base pressure is achieved, we place a shutter over the opening of the gate valve to reduce the pumping

| elements detected | ppm |
|---|---|
| Aluminum | 300 |
| Iron | 300 |
| Copper | 70 |
| Silicon | 70 |
| Calcium | 50 |
| Yttrium | 20 |
| Nickel | 20 |
| Magnesium | 10 |
| Silver | 1 |
| Manganese | <1 |

**Table 2.1** Elemental analysis of scandium sputter target – Results of elemental analysis of scandium sputter target, values given in parts per million.

speed, and high-purity argon is leaked into the chamber until the pressure rises to about $1 - 3$ mTorr [7].

The basic components within the vacuum chamber are the sputtering gun and target, and the sample holder with a substrate attached (see Fig 2.1). Once the desired pressure is reached, we turn on the power supply, bringing the sputtering gun and target to high negative voltage (approximately 0.4 kV) with respect to the grounded chamber. Argon atoms become ionized and form a plasma inside the chamber. These argon ions are accelerated towards the target by the negative bias. Collisions with atoms in the surface of the target dislodge atoms from the target and set them adrift. This allows the target atoms, scandium for this project, to be deposited on exposed surfaces in the chamber, including the substrate. For this project, we also introduce oxygen gas into the chamber to add oxygen atoms to the plasma and surrounding gas, forming scandium oxide on the substrate, rather than pure scandium [7]. We actually prefer working with oxidized films as they are more stable and therefore, easier to work with. This also serves to test methods of estimating the optical constants of materials from their constituent elements.

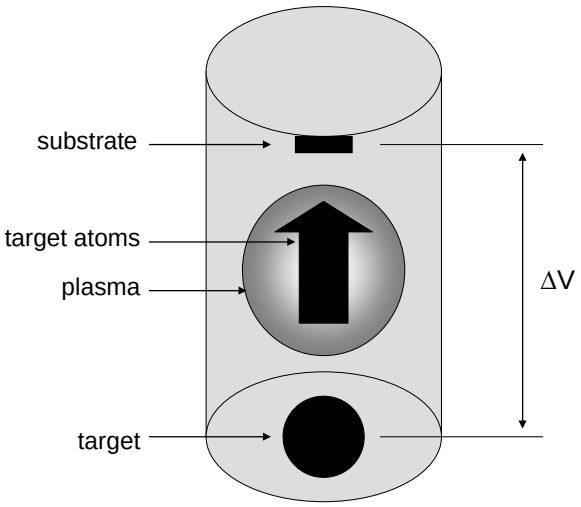


**Figure 2.1** Diagram of the sputtering process in a vacuum chamber – Atoms from the sputter target are dislodged by collisions with atoms from the plasma and deposited on the substrate.

The optical constants of the silicon and silicon dioxide layers found in photodiodes are well-characterized, making photodiodes a useful substrate for sputtering. A photodiode is designed to output an electrical signal when a photon is incident on its surface. Films sputtered directly on a photodiode facilitate the collection of transmission data from the film [3, 9]. These same films can also be used for reflection measurements if light reflected off the coated diode is collected by an uncoated diode.

The photodiodes we use in the Thin Films Group are model AXUV-100, manufactured by International Radiation Detectors, Inc [7]. These detectors, manufactured in a given batch, are presumably identical. However, the Thin Films Group has done studies of uncoated diodes from the same batch which showed that, even though responses versus wavelength were nearly identical over a broad spectral range ($5 - 18$ nm), differences of up to 5% were seen among the diodes at shorter wavelengths [7]. Therefore, we need to account for these differences by characterizing the response of each photodiode before coating. When measuring optical constants of films coated on these diodes, it is important to note that there is a layer of silicon dioxide $6.5 - 6.7$ nm

thick on the surface of the silicon photodiode. The thickness in this range was specified by the manufacturer as well as independently verified experimentally through ellipsometry by our group [3, 10].

Aside from knowing the thickness and density of the silicon and silicon dioxide of the photodiode, we also need to know both the thickness and density of the thin film for reflection and transmission measurements to be useful in calculating the optical constants of a material. In the Thin Films Group, we use ellipsometry to determine thickness and Transmission Electron Microscopy (TEM) to determine density.

## 2.2 EUV measurements at the ALS

The reflection and transmission measurements of the scandium thin films were made on Beamline 6.3.2 of the Lawrence Berkeley National Laboratory Advanced Light Source (ALS). The ALS is a synchrotron light source, which provides high-intensity light in the ultraviolet and soft-x-ray ranges. Beamline 6.3.2 in particular, constructed by the Center for X-Ray Optics (CXRO), is designed to provide light with high spectral purity and wavelength accuracy. The key components of the beamline (see Fig 2.2) are the variable-line-spaced plane gratings, the filters (not shown) and the order suppressor, which together provide the high spectral purity and wavelength accuracy. Each specific combination of grating, filter, and order suppressor allows access to only a small range of wavelengths. However, it is possible to access wavelengths from $2.7 - 50$ nm on the beamline. Data can be obtained over the full range of wavelengths by collecting data over each small range successively and combining the results.

Reflection and transmission measurements can be taken simultaneously through the use of two diodes, one coated and one uncoated. The AXUV-100 photodiodes used for these measurements have increased sensitivity in the EUV range [9]. When

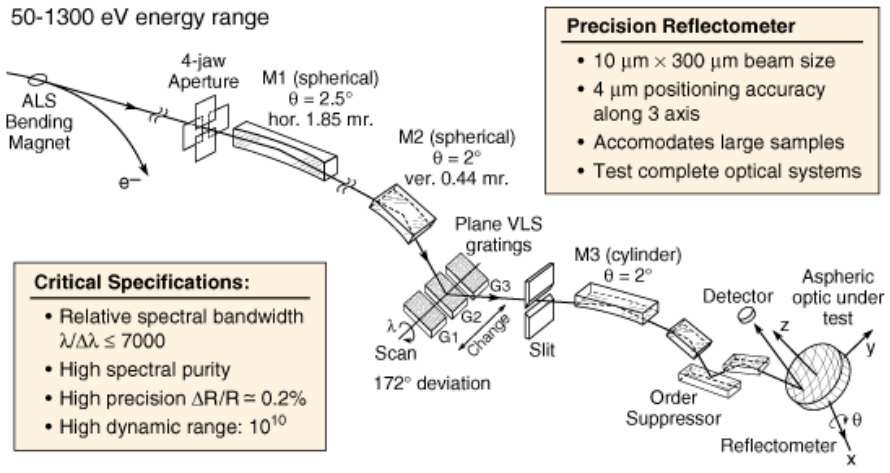


**Figure 2.2** Schematic of ALS beamline 6.3.2 – Schematic of ALS beamline 6.3.2 taken from http://www-cxro.lbl.gov/als6.3.2/

light is incident on a coated diode, there are three possible paths for it to follow. Incident light can be transmitted through, reflected from, or absorbed in the coating (see Fig 2.3). Using coated diodes has made the transmission measurement more practical by placing the thin film directly between the detector and the incident light. Use of a second, uncoated, diode enables the reflection measurement by allowing the collection of light reflected off the surface of the film. This diode is a permanent part of the beamline and is also an AXUV-100, but from a different batch.

To allow for measurements at angles less than 25°, referred to as near-grazing, Guillermo Acosta of the Thin Films Group designed a stage to hold a coated photodiode without blocking light incident at these angles. The stage also holds an additional AXUV-100 diode, also uncoated, to simplify calculations of optical constants [7]. The positioning system already in use in the vacuum chamber of Beamline 6.3.2 allows the diode being studied to be rotated to any angle, while the reflection detector is simultaneously positioned at twice that angle. This system also allows the sample stage to be positioned in three dimensions with a precision of 4 $\mu$m [11].

The easiest way to collect data at the ALS is to measure reflection and transmission

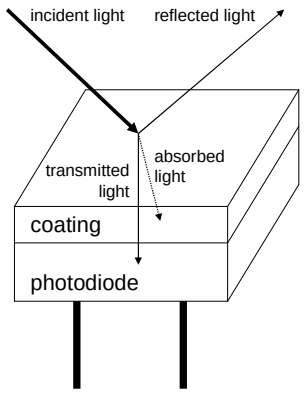


**Figure 2.3** Possible paths for incident light – Light incident on a coated diode can either be reflected off the coating, absorbed by the coating, or transmitted through the coating to the photodiode underneath.

for a range of wavelengths at a single angle. Because the optical constants of the materials involved will be different for each wavelength, it is most convenient to have data at a single wavelength for a range of angles. Data of this sort can be collected by measuring the reflection and transmission for a batch of single angles over the range of wavelengths. We run this data through a computer program that breaks the data down into wavelength-angle pairs and reconstructs individual data sets of reflection and transmission as a function of angle for each wavelength.

Once the data set is in a more usable form, it must still be normalized before optical constants can be computed. Normalization converts the data from relative reflection and transmission to absolute reflection and transmission. The first step in normalizing the data is to subtract off the gain-specific dark current. Each measurement is taken at a specific gain setting (amplification of the signal), and a dark signal measurement taken with no incident light is also taken for each gain setting. Subtracting the dark current ensures that the data being used represent only the photons that come from the monochromator beam at the ALS. Then the reflection and transmission measurements are divided by the ALS beam current from that measurement, as the current varies with each measurement. Additionally, these values are divided by

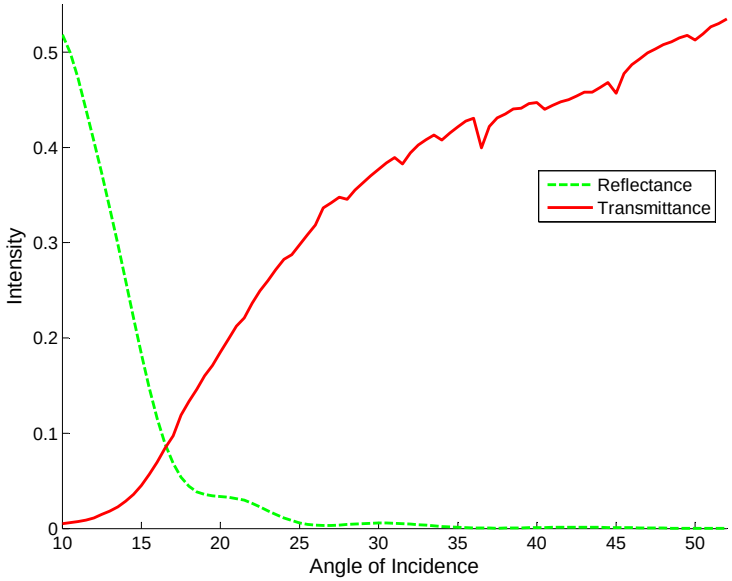


**Figure 2.4** Normalized reflectance and transmittance data – Reflectance and transmittance data that has been normalized using Eq. (2.1).

a factor that represents the absolute intensity of the unobstructed full beam. These values are then divided by an additional scaling term that takes into account the different gains used for full beam intensity data and reflection and transmission data. The equation below represents the normalization equation for reflection [7]:

$$R_{normalized} = \frac{\frac{Signal_R - DarkCurrent_R}{BeamCurrent_R}}{\frac{Signal_{FB} - DarkCurrent_{FB}}{BeamCurrent_{FB}} 10^{Gain_R - Gain_{FB}}}. \tag{2.1}$$

The subscript $R$ stands for reflection and the subscript $FB$ stands for full beam. (Transmission is normalized with a similar equation.) An example of normalized reflectance and transmittance data can be seen in Fig. 2.4. As would be expected, reflectance decreases and transmittance increases as the angle from grazing increases towards normal incidence. It is important to note that reflectance varies more with angle than transmittance does.

After the data set has been normalized, it is possible to calculate, $\delta(\omega)$ and $\beta(\omega)$, the real and imaginary parts of the complex index of refraction. However, it is significantly more difficult to calculate the real part $\delta(\omega)$ as it requires use of both

reflectance and transmittance data. It is possible to calculate the imaginary part $\beta(\omega)$ from only the transmission data because this property varies slowly with angle. Applying KK analysis to this experimentally determined $\beta(\omega)$ should produce a $\delta(\omega)$ that reasonably matches the experimentally calculated values.

Along with other members of our research group, I traveled to the ALS to measure reflectance and transmittance. Acosta used this data to calculate delta and beta by the above mentioned method. His calculations (those referred to as RT calculations) can be found in his dissertation [7] and are the basis for my own calculations.

# Chapter 3

# Data analysis and discussion

Although Kramers-Kronig analysis (KK) is most useful when performed on experimental data, we chose to test it first on generated data. Generating $\beta$ data, for which we know the $\delta$ counterpart, allows us to see if we are doing the analysis properly. As we wanted to see how well our method works for data similar to the experimental data we would like to analyze, we chose to begin by doing KK on $\beta$ values, provided by CXRO [12].

Once we verified that our method was reasonably able to reproduce CXRO $\delta$ values from CXRO $\beta$ values, we performed the analysis on smaller sections of CXRO values to see the effects that limiting wavelength range has on the accuracy of KK analysis. We also tested the effects of increasing and decreasing the density of points in the data. After we understood the behavior of KK analysis with different sets of data, we were able to test it on experimental data.

## 3.1 Analytic method

The Kramers-Kronig relations seen in Eqs. (1.1)-(1.4) are meant to be used on equations, rather than sets of numerical data. The equations for $\delta$ and $\beta$ still apply, but to use the KK relations on our data, we needed to change the equations from integrals to summations. By changing $du$ to $\triangle u$, the integral can easily be converted to a sum. The original equation:

$$f_1^0(\omega) = Z - \frac{2}{\pi} P_C \int_0^\infty \frac{u f_2^0(u)}{u^2 - \omega^2} du \tag{3.1}$$

becomes

$$f_1^0(\omega) = Z - \frac{2}{\pi} \sum \frac{u f_2^0(u)}{u^2 - \omega^2} \triangle u \tag{3.2}$$

where $u$ is energy. The arguments of these summations can be evaluated on a point-by-point basis and summed to parallel the integrals in the original equations. To avoid a singularity, we do not include the points for which $u^2 - \omega^2 \approx 0$. The code used for our analysis can be found in Appendix A.

## 3.2 Analysis of CXRO data

Values provided by CXRO include both the real and imaginary parts of the index of refraction for a specified material over a finite range. Each set of CXRO values corresponds to a specific user defined density of the given material. The values of these data were calculated through a combination of theory and KK analysis. Therefore, by performing KK analysis on the imaginary part of the CXRO values, we should be able to replicate successfully the real part. The difference between the CXRO values of $\delta$ and those from KK analysis for scandium oxide (for a chosen density of 3.4 g/cm$^3$) can be seen in Figs. 3.1 and 3.2. The feature present in $\delta$ around 400 eV resulted in high amplitude oscillations in the percent difference between the KK

$\delta$ and the $\delta$ provided by CXRO. We also note that the percent error is significantly smaller at high energy, where there are no absorption features.

Our experimental data only cover an energy range of about 40 eV to 270 eV, causing our summations to only be approximate. Therefore, we chose to investigate the effect of not having a broader energy range. A test on truncated sets of data reveals that KK analysis is most accurate on sets of data that cover the broadest range of energy. Aside from the obvious trend for KK analysis to lose accuracy as the range of data being used is shortened, it is also important to note that the ends of each set of data have a high error. This, however, should be expected. We are applying an equation that is meant to be used over an infinite range of data to a finite range of data. However, we see that when using the available CXRO values, which do not cover the entire EUV range, we are able to calculate $\delta$ to within 1% of the CXRO values (see Fig. 3.3). The range for which we measure experimental data is even shorter than the smallest range shown in Fig. 3.4, which had an error of over 60%. We are, therefore, able to conclude that small ranges of data must be augmented with synthetic values values to achieve realistic results from KK.

Tests on data sets with a decreased number of data points covering the same energy range of data, show that the number of points in our case does not affect the accuracy of KK analysis substantially until the number of points is reduced to about 10% of its original number (as seen in Figs. 3.5 and 3.6). The experimental data we collect will always be more dense than 50 points over 30000 eV, so the density of points should not be a problem in our KK analysis. Since reducing the density of the points had little effect on the calculation, it follows that it would be unnecessary to choose a sophisticated integration process such as Simpson's rule over a simple point-by-point summation (skipping over singularities).

Another key factor in the accuracy of KK analysis is the density term in Eqs.

(1.1) and (1.2), which relate $\delta(\omega)$ and $\beta(\omega)$ to $f_1^0(\omega)$ and $f_2^0(\omega)$. The values provided by CXRO corresponds to a given density. Therefore, if the density used in the KK analysis doesn't match the density used to generate the CXRO values, the calculated $\delta$ values will not match the values provided by CXRO. When data values are available at high energies, it is easy to identify the right density. A feature of the real part of the atomic scattering factor $f_1$ is that at high energy it approaches $Z$, the effective charge of the material in question. We used $Z = 33$ for scandium oxide in our program, which was obtained by adding $Z(Sc) = 21$ and $Z(O_{1.5}) = 12$. These values for $Z$ are the result of the stoichiometry ($ScO_{1.5}$) and density that we used to obtain CXRO values. Had we chosen to use $Sc_2O_3$ for our stoichiometry, Z would have been 66. Figures 3.7 and 3.8 show $f_1$ calculated for various density values on a single file. The density used to create the CXRO values is 3.4 g/cm$^3$. When KK analysis is given a density less than 3.4 g/cm$^3$, $f_1$ approaches a value greater than $Z$. When the density used in KK analysis is greater than 3.4 g/cm$^3$, $f_1$ approaches a value less than $Z$. However, when the correct density is used, $f_1$ approaches $Z$ as energy approaches infinity. This means that if data values are known at high energy but the density is unknown, it is possible to recover the density by testing different densities to see which density results in an $f_1$ that approaches $Z$ as energy increases.

## 3.3 Analysis of ALS data

With an understanding of the operation of Kramers-Kronig analysis on theoretical data, it is possible to use it also on $\beta$'s calculated from reflection and transmission measurements, which we will call RT data. We discovered that two things are necessary for Kramers-Kronig analysis to be successful: smoothing of the data set and augmentation with values from CXRO. The latter must be done to provide reasonable

values of $\beta$ in the range where measurements were not made to make the sums more complete.

An initial run of the analytic program reveals that experimental RT data must be smoothed for KK analysis to yield a smooth $\delta$. Figure 3.9 shows a section of the $\delta$ calculated by KK analysis on the $\beta$ data calculated from reflection and transmission. This section shows a problem that arises in areas where the data points do not form a smooth line. After we manually smooth the RT data, KK analysis yields a much cleaner, smoother line (see Fig. 3.10). Although smoothing the data by a more automated process would have been more repeatable, such a process is outside the scope of this project, as only one data set is under study. For obvious reasons, the summation used in KK analysis works better on smooth data than on rough data.

Our motivation for testing this analysis was to come up with an easier, more accurate way to calculate $\delta$ for thin films. As we are not completely satisfied with our current method of calculating $\delta$, we don't expect our KK $\delta$ to exactly match our previously calculated values, nor do we expect our calculation to exactly match the theoretical values provided by CXRO, which doesn't take into consideration chemical bonding effects. When we apply KK analysis, truncating the sums to include only our experimental data, the resulting difference between our KK calculation and our RT calculation is over 100%, and the KK $\delta$ does not match the CXRO values any closer than this. A plot of the KK results overlayed with the CXRO and RT calculated values can be seen in Fig. 3.11.

These results support our hypothesis that it is necessary to extend the range of the data being analyzed by attaching CXRO values at both ends of our experimental data. This more nearly completes the summation, providing greater accuracy. However, we need to know what density to use for scandium oxide in our calculations. Each set of CXRO values corresponds to a single density. Both the KK $\delta$ and the CXRO $\delta$ are

different for each density used in KK analysis, but the RT $\delta$ calculated by Acosta in his dissertation does not depend on density [7]. Decreasing the density used in the calculation, which requires using a different set of CXRO values, lowers the entire $\delta$ for both KK and CXRO. If we use CXRO values based on the wrong density, our KK analysis will not work as well as it should. Unfortunately, the exact density of thin films is not always known. The optical constants of compound materials, such as scandium oxide, are most often compiled assuming bulk density (3.86 g/cm$^3$ for scandium oxide). A good assumption, therefore, would be that this density should be used in KK analysis. However, we would prefer to test the effects of using different densities to determine if this is the correct density, but first we need to explore the effects of roughness. (For a more detailed explanation of the calculation of optical constants of compound materials, see Appendix B.)

At high energies wavelengths are shorter, causing light to be more easily scattered by the roughness of the surface, allowing less of the reflected light to be collected by the detector. The effects of roughness in the EUV is an area of active research [13–15], including work done in past and present theses of our group [16–18]. Due to the increase in scattering from rough surfaces at these higher energies, we expect our KK calculation to yield larger values of $\delta$ than those calculated from reflection and transmission measurements because, this method currently does not take into account the effects of roughness. A $\delta$ calculated from the RT data would underestimate the KK $\delta$ in areas where scattering occurs because the KK relations are based on $\beta$, which comes from transmission and is not strongly affected by roughness scattering. Therefore, we expect the $\delta$ from our KK calculation from $\beta$ could be greater than that from reflection and transmission calculations.

Aside from expecting our KK calculation could be greater than the values calculated from reflection and transmission (unless the sample used in RT measurements

were extremely smooth), we also expect our calculation to match these values more closely at lower energies, where scattering is less of a factor, and to match CXRO closely away from absorption features, which in this study at higher energies. With decreasing energy, scattering becomes less of a problem and we expect our calculation to converge with the values calculated from reflection and transmission data.

Returning to the issue of density, Figs. 3.12 and 3.13 show the results of KK analysis using two different densities, bulk density (3.86 g/cm$^3$) and a lower density (3.2 g/cm$^3$). The only density that gives us a $\delta$ that is greater than the RT data at low energies and closely matches CXRO values at higher energies was 3.86 g/cm$^3$, which corresponds to 100% dense scandium oxide. An example of a density that does not give satisfactory results is seen in Fig. 3.13. The $\delta$ calculated using KK analysis on this density is lower than Acosta's RT calculation from reflection and transmission data and follows neither CXRO nor the values calculated from reflection and transmission at the higher energies. These results lead us to believe that our scandium oxide thin film is close to 100% dense.

The results of KK analysis on our RT $\beta$ data using 100% density (3.86 g/cm$^3$) differ from the $\delta$ calculated from reflection and transmission data by less than 50% across the entire range of measured data. The percent difference between the KK $\delta$ values and RT values seen in Fig 3.14 is negative because the KK values are greater than those calculated from reflection and transmission data. At the higher energies, the magnitude of the percent difference increases significantly. This is the area in which we expect our calculation to follow the CXRO values more closely than the $\delta$ calculated from reflection and transmission data due to roughness scattering effects. Figure 3.15 shows that in this area the KK $\delta$ differs by a smaller percent from the CXRO values than from the RT values.

## 3.4 Conclusions

I have determined the $\delta$ of scandium oxide from 40 to 270 eV via KK analysis. This $\delta$ matches CXRO values quite closely except in regions with high absorption where it is expected to differ because of chemical shifts. The results of my computational analysis show that the $\delta$ calculated from reflection and transmission data without taking into account roughness may underestimate $\delta$ by up to 40% near 270 eV (see Figs. 3.14 and 3.15. It is noteworthy that these KK calculations more closely match the values provided by CXRO in the areas where they least match the RT calculations, as expected. For this method of calculating $\delta(\omega)$ to be accurate, it is necessary to smooth the experimental data and determine the density of the thin film being measured.

To make KK analysis more accurate in the entire EUV range, we need to find a way to obtain data for the lower energies in the range. Currently, CXRO only provides values down to 30 eV and we are only able to obtain clean experimental data down to about 41 eV. Adding CXRO values to the low energy end of our experimental data doesn't extend the range by very much, creating extra error at the low energy end of our KK analysis. Another way to reduce the difference between the $\delta(\omega)$ calculated by our other method and that calculated by KK analysis is to account for the scattering of light due to roughness in our reflection and transmission method of calculating $\delta$ and $\beta$.

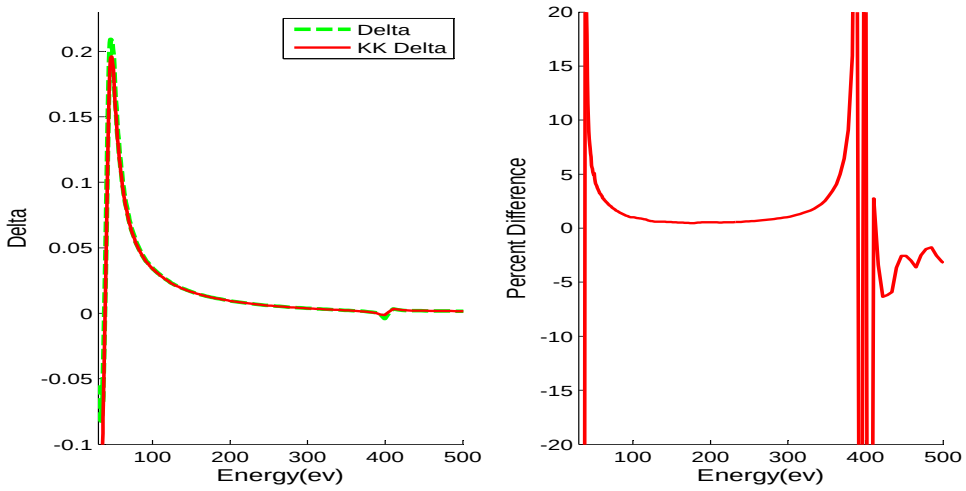


**Figure 3.1** Kramers-Kronig analysis on CXRO data at low energy – Plot of the $\delta$ resulting from Kramers-Kronig analysis on CXRO $\beta$ data at low energy (calculated using data from 30 eV to 30 keV). The graph on the left shows the CXRO calculation of $\delta$, as well as our KK calculation of delta. The graph on the right shows the percent difference between the two. At low energies, the percent difference is reasonable, but significant.

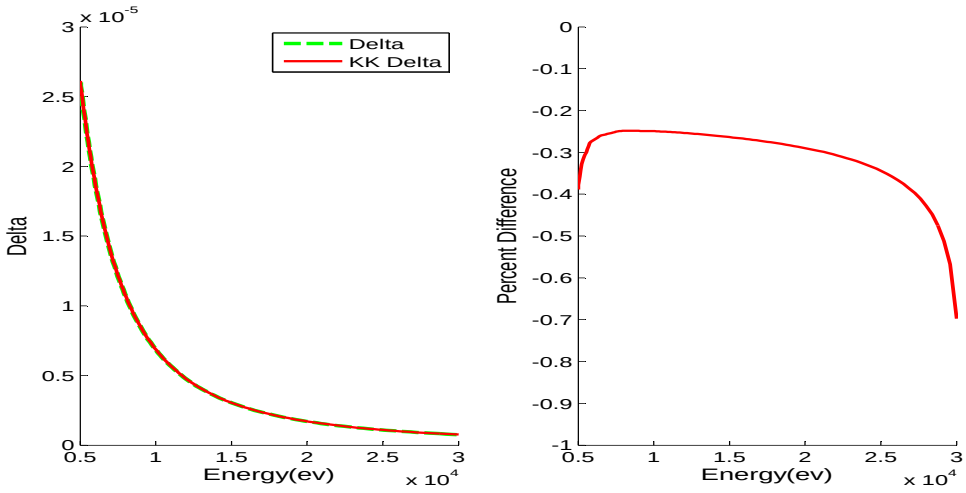


**Figure 3.2** Kramers-Kronig analysis on CXRO data at higher energy –Plot of the $\delta$ resulting from Kramers-Kronig analysis on CXRO $\beta$ data at higher energy (calculated using data from 30 eV to 30 keV). The graph on the left shows the CXRO calculation of $\delta$, as well as our KK calculation of delta. The graph on the right shows the percent difference between the two. Note that the difference is much less than 1% in this range.

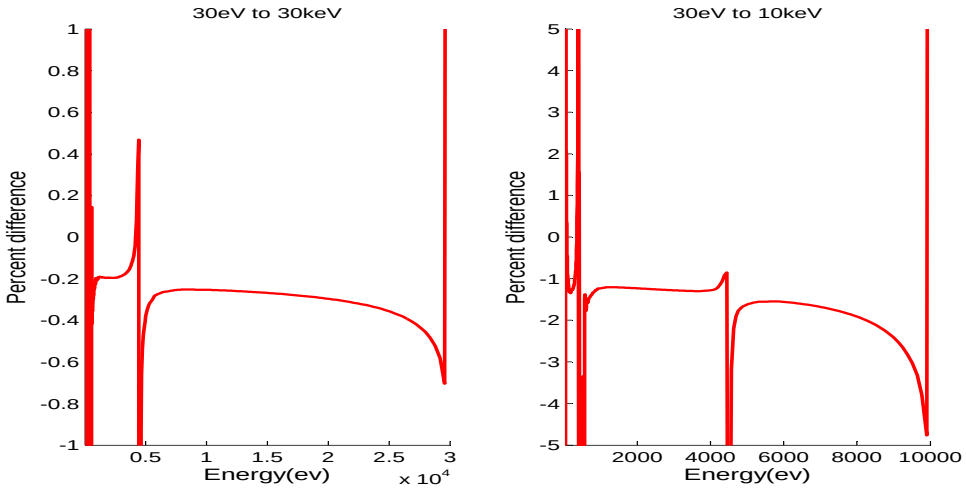


**Figure 3.3** Truncated data sets – Plots of KK analysis are represented in the form of a percent difference between the KK calculation and the value provided by CXRO. The percent difference increases when the range of data being analyzed in the KK sums is shortened. This is particularly true near the ends of the ranges.

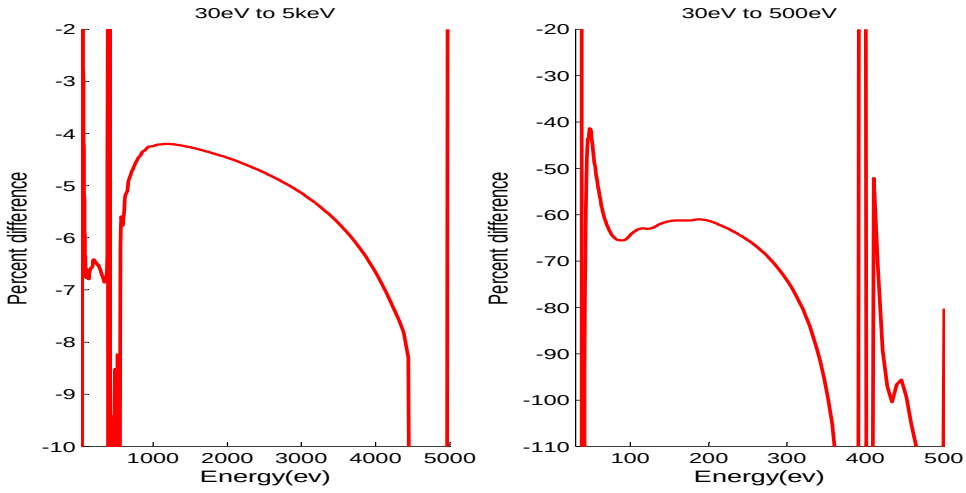


**Figure 3.4** Truncated data sets – Additional plots of KK analysis are represented in the form of a percent difference between the KK calculation and the value provided by CXRO. The percent difference increases when the range of data being analyzed in the KK sums is shortened. This is particularly true near the ends of the ranges.

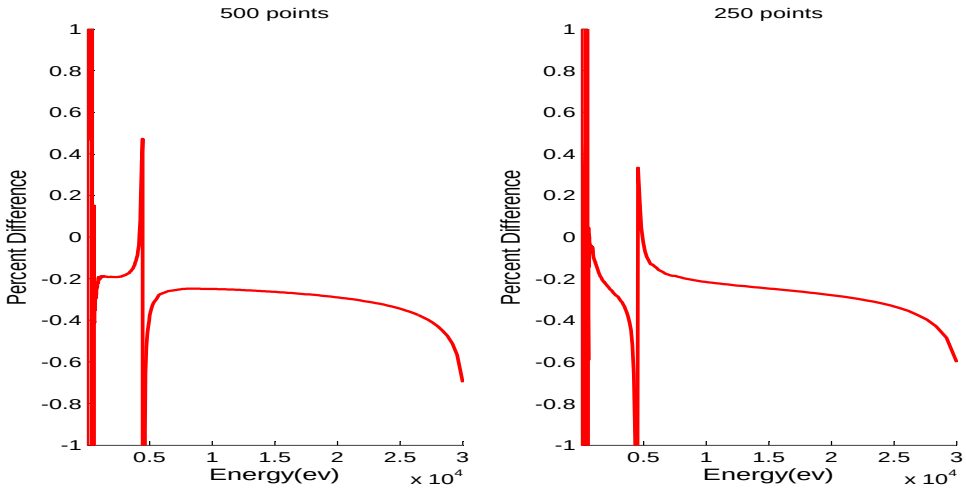


**Figure 3.5** Percent difference for 500 and 250 points – The effects of reducing the number of $\beta$ values in the KK sums to calculate $\delta$. The results of KK analysis are represented in the form of a percent error between the KK calculation and the value provided by CXRO. The percent error is similar for 500 and 250 data points.

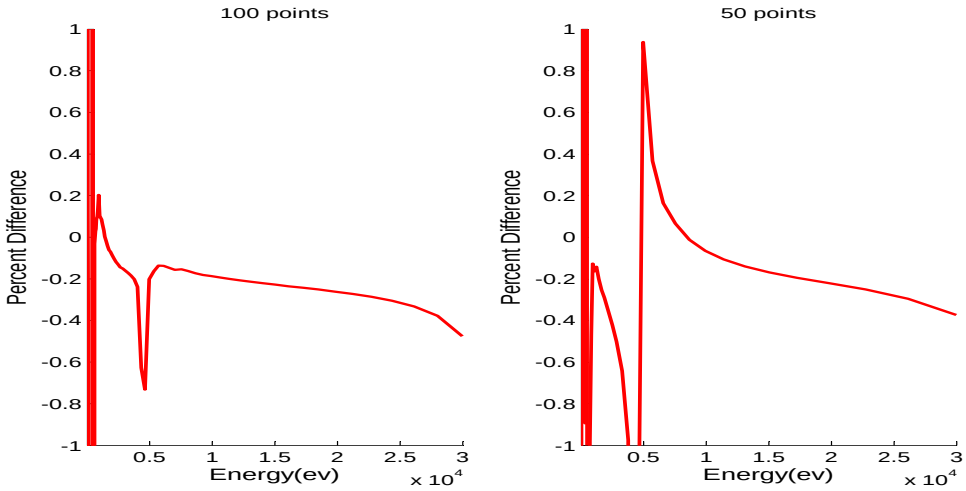


**Figure 3.6** Percent difference for 100 and 50 points – The effects of reducing the number of $\beta$ values in the KK sums to calculate $\delta$. The results of KK analysis are represented in the form of a percent error between the KK calculation and the value provided by CXRO. The percent error is less stable for fewer data points.

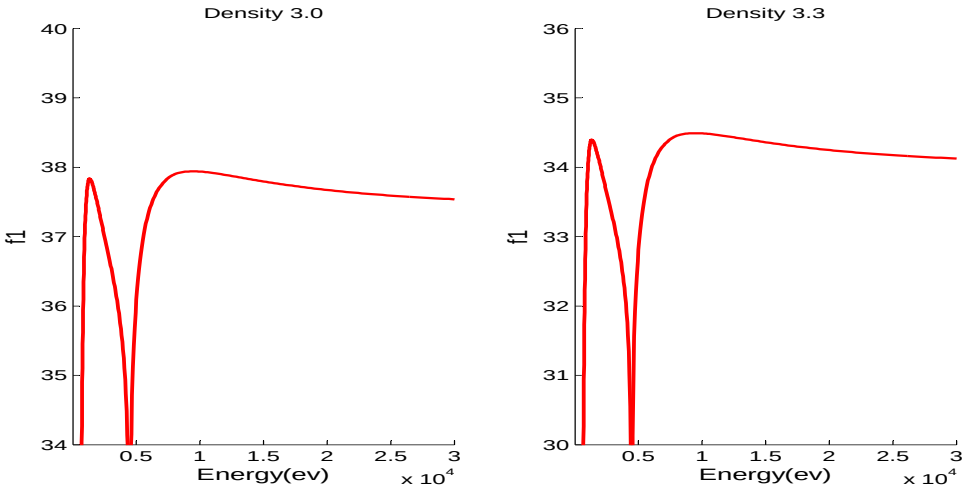


**Figure 3.7** $f_1$ for densities of 3.0 and 3.3 g/cm$^3$ – For both of these densities, $f_1$ approaches a value greater than 33 as energy approaches infinity.

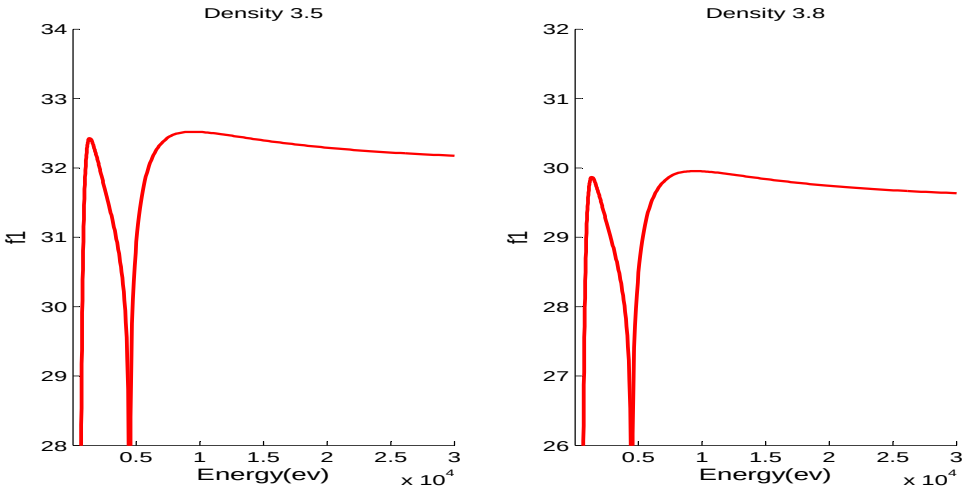


**Figure 3.8** $f_1$ for densities of 3.5 and 3.8 g/cm$^3$ – For both of these densities, $f_1$ approaches a value less than 33 as energy approaches infinity.

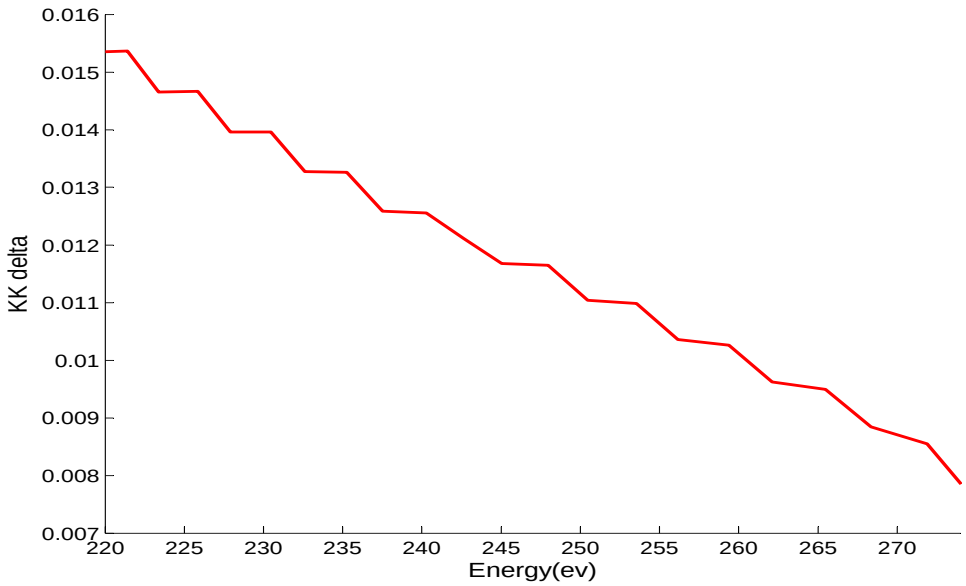


**Figure 3.9** Results of KK analysis on unsmoothed data – Before the $\beta$ data have been smoothed, KK analysis yields "stair step" type artifacts.

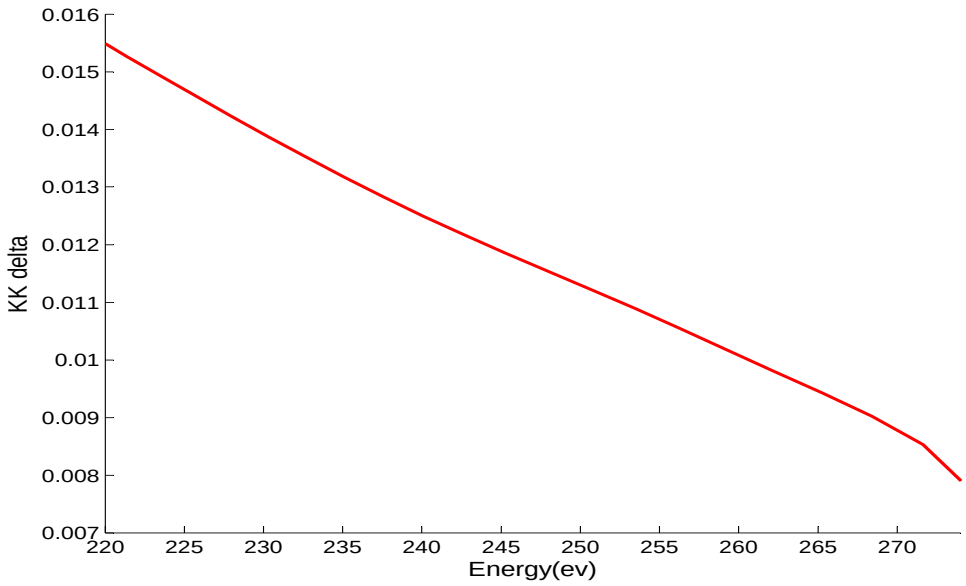


**Figure 3.10** Results of KK analysis on smoothed $\beta$ data – After the values of $\beta$ are smoothed, KK analysis gives smooth results.

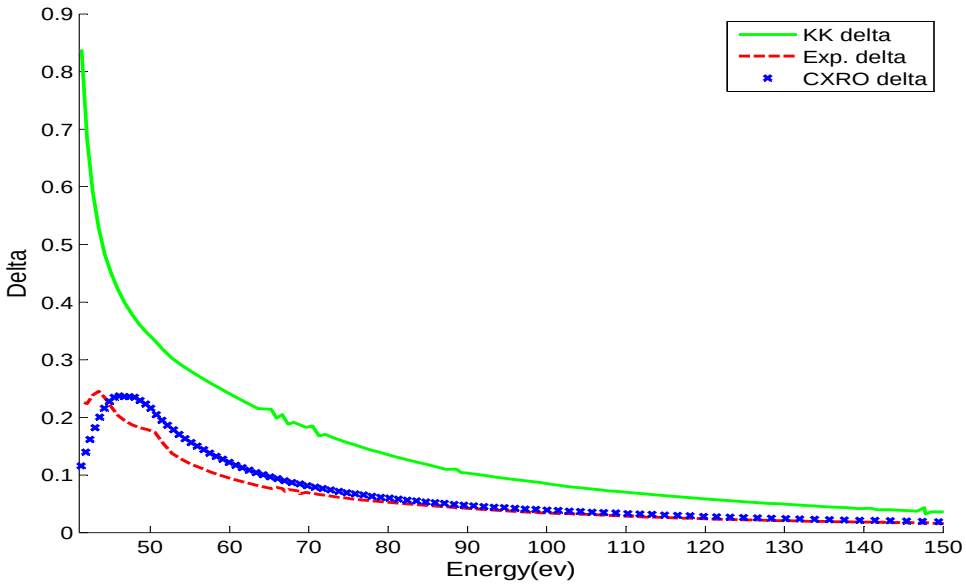


**Figure 3.11** Comparison of KK analysis with experimental data and CXRO data – We can see that as energy increases, CXRO and our experimental values converge, but the KK values (the solid line) are about twice as high as the other values.

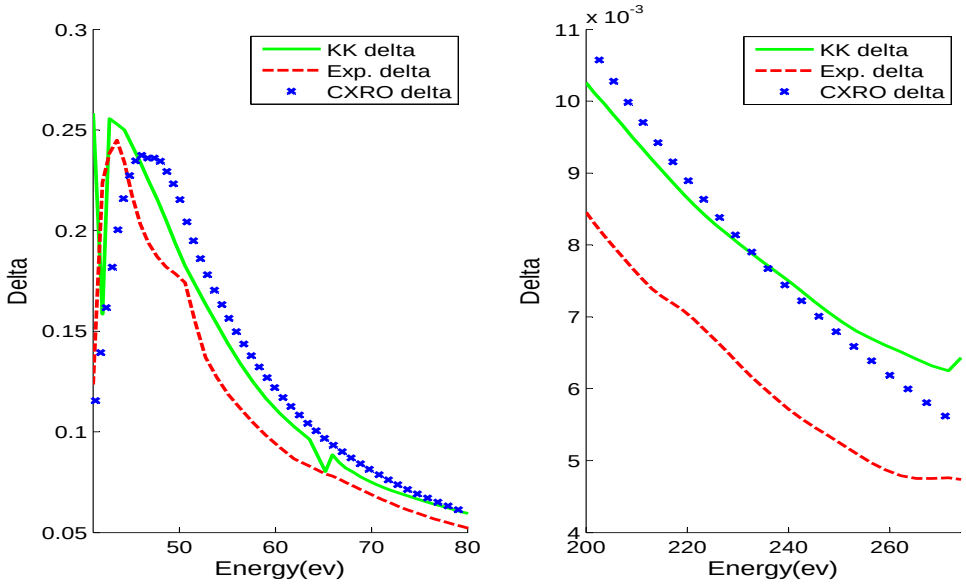


**Figure 3.12** Results of KK analysis for density of 3.86 g/cm$^3$ – For this density, the KK calculation is greater than the experimental calculation, but with a similar shape, at lower energies and matches CXRO values more closely at higher energies.

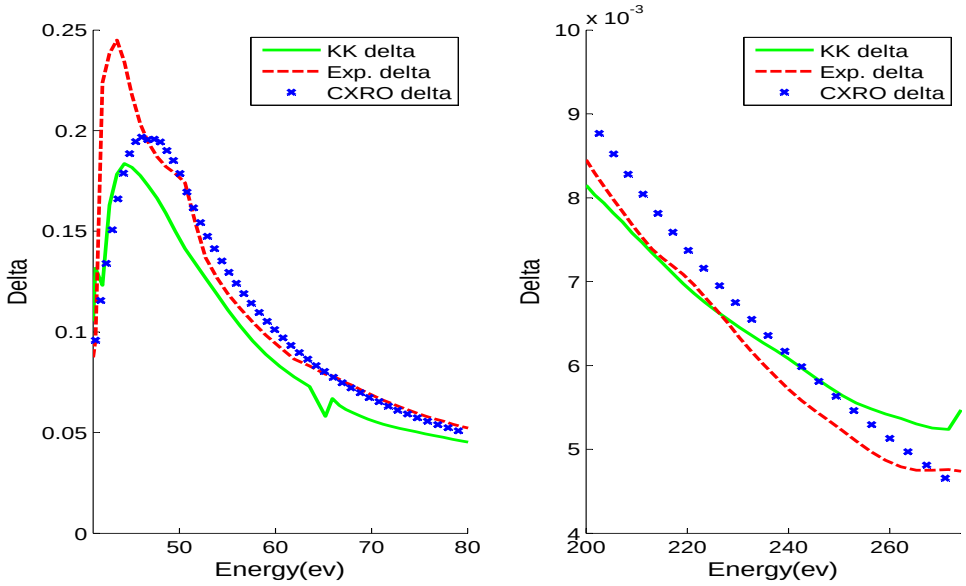


**Figure 3.13** Results of KK analysis for density of 3.2 g/cm$^3$ – For this density, the KK calculation is less than the experimental calculation, but with a similar shape, at lower energies and follows neither CXRO nor experimental values at higher energies.

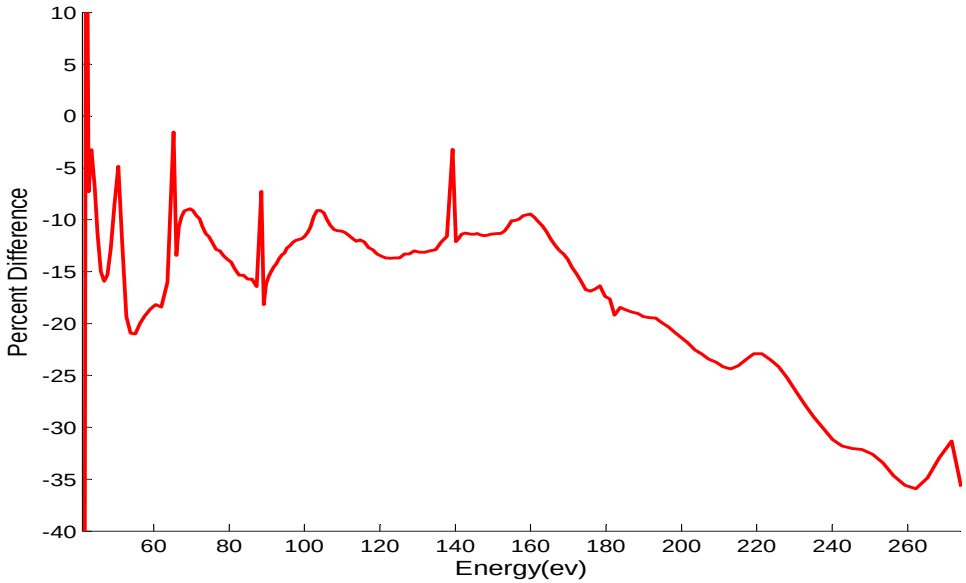


**Figure 3.14** Percent difference between KK results and experimental data – We can see that as energy increases, our calculation differs increasingly with the experimental data. The negative sign on the percent difference shows that our KK values our greater than the experimental values.

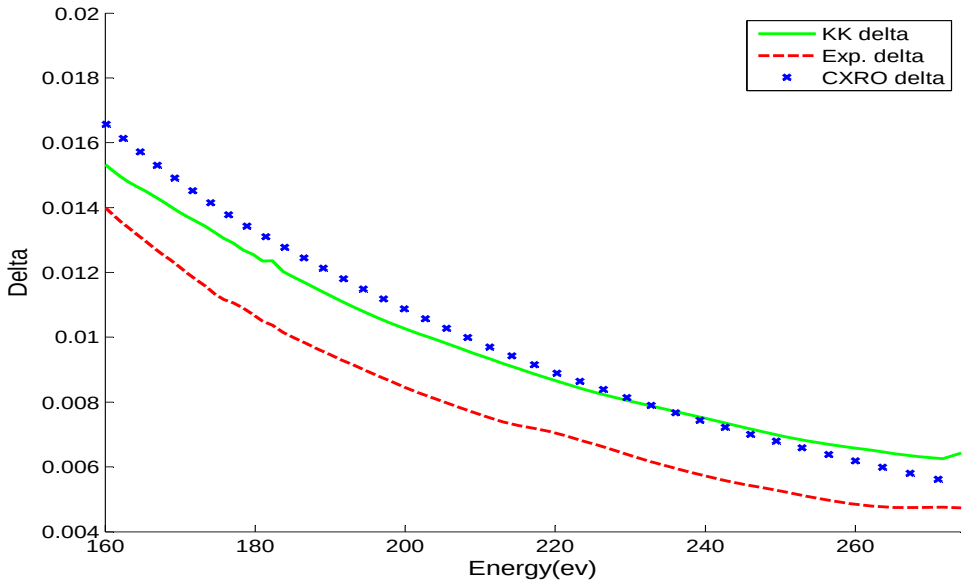


**Figure 3.15** Results of KK analysis on experimental data at higher energies – In this range, where the percent difference with the experimental data was greater, we can see that the difference between the KK results and the CXRO data is smaller.

# Bibliography


[1] *http://pluto.space.swri.edu/IMAGE/payload.html* (Accessed February 2007).

[2] Y. A. Uspenskii, V. E. Levashov, A. V. Vinogradov, A. I. F. V. V. Kondratenko, Y. P. Pershin, E. N. Zubarev, and V. Y. Fedotov, "High-reflectivity multilayer mirrors for a vacuum-ultraviolet interval of 3550 nm," Optics Letters **23,** 771–773 (1998).

[3] Y. A. Uspenskii, J. F. Seely, N. L. Popov, A. V. Vinogradov, Y. P. Pershin, and V. V. Kondratenko, "Efficient method for the determination of extreme-ultraviolet optical constants in reactive materials: application to scandium and titanium," J. Opt. Soc. Am. A **21,** 298–305 (2004).

[4] S. A. Korff and G. Breit, "Optical Dispersion," Rev. Mod. Phys. **4,** 471–503 (1932).

[5] G. B. Arfken and H. J. Weber, *Mathematical Methods For Physicists, 6th Ed* (Elsevier Academic Press, Burlington, MA, 2005).

[6] D. T. Attwood, *Soft x-rays and extreme ultraviolet radiation : principles and applications* (Cambridge University Press, Cambridge, UK, 2000).

[7] G. Acosta, "Scandium Oxide Thin Films and Their Optical Properties in the Extreme Ultraviolet," PhD Dissertation, Dept. of Physics and Astronomy, Brigham Young University (2007).

[8] A, *First Reaction Product Spec Sheet for* 4" *Scandium Sputter Target* (First Reaction, Depot Road, Hampton Falls, New Hampshire, 37).

[9] E. M. Gullikson, R. Korde, and R. E. Vest, "Stable silicon photodiodes for absolute intensity measurements in the VUV and soft x-ray regions," J. electron spectrosc. relat. phenom. **80,** 313–316 (1996).

[10] A. L. Aquila, F. Salmassi, E. M. Gullikson, F. Eriksson, and J. Birch, "Measurements of the optical constants of scandium in the 50-1300 eV range," University of California eScholarship Repository **LBNL-58403,** 1–9 (2004).

[11] *http://www-cxro.lbl.gov/als6.3.2/* (Accessed February 2007).

[12] *http://www-cxro.lbl.gov/optical_constants/getdb2.html* (Accessed February 2007).

[13] D. G. Stearns and E. M. Gullikson, "Nonspecular scattering from extreme ultraviolet multilayer coatings," Physica B **283,** 84–91 (2000).

[14] D. G. Stearns, "X-ray scattering from interfacial roughness in multilayer structures," J. Appl. Phys. **71,** 4286–4298 (1992).

[15] D. L. Windt, "IMd - Software for modeling the optical properties of multilayer films," Computers in Physics **12,** 360–370 (1998).

[16] E. Martin, "Fill in later," Senior Thesis, Dept. of Physics and Astronomy, Brigham Young University (2007).

[17] N. Farnsworth, "Thorium-based Mirrors in the Extreme Ultraviolet," Honors Thesis, Dept. of Physics and Astronomy, Brigham Young University (2005).

[18] J. E. J. Johnson, "Thorium Based Mirrors for High Reflectivity in the EUV," Honors Thesis, Dept. of Physics and Astronomy, Brigham Young University (2004).

# Appendix A

# Kramers-Kronig analysis code

The Kramers-Kronig relations found in Chapter 1 are implemented in the following code:

```
clear; close all;
% Open a file containing CXRO and smoothed experimental
fid=fopen('dens386.txt'); dens=3.86;
% The first line of the file is a header, labeling the columns and is
% skipped over by the following line of code
textscan(fid, '%*s %*s %*s', 1, 'delimiter', '\t');
% Read the 3 columns of data into appropriately named arrays
data=textscan(fid,'%f %f %f', 'delimiter', '\t');
lambda=data{1,1}; delta=data{1,2}; beta=data{1,3}; fclose(fid);
% This term is used to convert wavelength (m) to energy (eV) and energy
% to wavelength
etolambdafactor=.000001239842;
% The classic electron radius
r0=2.81794e-15;
```

```
% Avagadro's number
NA=6.022136e23;
% Define the number of data points in the arrays (they all should be the
% same length)
N=length(lambda);
% Define the effective charge
Z=33;
% Define energy, f1, and f2 for each point in the data set
for n=1:N
    energy(n)=etolambdafactor/lambda(n);
    const(n)=(2*pi*137.91/2)/(NA*(dens*10^6)*r0*lambda(n)*lambda(n));
    f1(n)=delta(n)*const(n);
    f2(n)=beta(n)*const(n);
end
% rotate the arrays if desired
const=const';
f1=f1';
f2=f2';
% This nested loop does the summation and calculates f1 for each point
% in the array
for m=1:N
    % Initialize the sum to 0 for each point the loop is run for.
    sum(m)=0;
    % The 'if' statements keep the program from attempting to divide by
    % zero by setting the integrand to 0 for those terms
    if isequal((energy(1))^2-(energy(m))^2,0)
```

```
    integrand(1)=0;
else
    integrand(1)=f2(1)*energy(1)/((energy(1))^2-(energy(m))^2)
    *(energy(2)-energy(1));
end
if isequal((energy(N))^2-(energy(m))^2,0)
    integrand(N)=0;
else
    integrand(N)=f2(N)*energy(N)/((energy(N))^2-(energy(m))^2)
    *(energy(N)-energy(N-1));
end
% Add the integrands for the end terms together.
sum(m)=sum(m)+integrand(1)+integrand(N);
% Calculate the integrand for the points other than the end points
for n=2:N-1
    if isequal((energy(n))^2-(energy(m))^2,0)
        integrand(n)=0;
    else
        integrand(n)=f2(n)*energy(n)/((energy(n))^2-(energy(m))^2)
        *(energy(n+1)-energy(n-1))/2;
    end
    % Add up the integrand from these points
    sum(m)=sum(m)+integrand(n);
end
% Use the sum to calculate f1 for a different point each time the
% loop is run
```

```
    f1calc(m)=Z-(2/pi)*sum(m);
end
f1calc=f1calc';
% Calculate delta from f1 and find a percent difference between the new
% and original delta
for n=1:N
    deltacalc(n)=f1calc(n)/const(n);
    diff(n)=delta(n)-deltacalc(n);
    pdiff(n)=(diff(n)/delta(n))*100;
end
diff=diff';
deltacalc=deltacalc';
pdiff=pdiff';
```

# Appendix B

# Compilation of optical constants for compound materials

The optical constants for compound materials for which the optical constants have not been experimentally measured and published, such as scandium oxide, are compiled from data for the elements of which it is composed. The optical constants for both scandium and oxygen have been experimentally measured and are available for use. To determine synthetic values for the optical constants of scandium oxide, the optical constants of the elements must be converted to atomic scattering factors. This conversion requires dividing the optical constants by the factor,

$$C = \frac{n_a r_e \lambda^2}{2\pi}, \tag{B.1}$$

where $n_a$ is the number of atoms per unit volume in the optical medium and $r_e$ is the classical electron radius. The combination of the stoichiometry and density of a material, determines its atomic density. When converting optical constants of elements to atomic scattering factors, bulk density is assumed unless otherwise stated. Atomic scattering factors for multiple elements can be used to determine the atomic scattering factors of a compound, providing it has a known stoichiometry. Once the

atomic scattering factors for a compound have been calculated, they can be converted back to optical constants by multiplying by $C$ (where $n_a$ is the atomic density of the compound material this time). The CXRO database that provides optical constants for compounds, requires the user to input a density and a stoichiometry [12]. These values are then used to calculate $n_a$ and optical constants are calculated and provided for that particular value of $n_a$.

# Index